Desalination and Water Treatment
www.deswater.com
43 (2012) 291–297
April
1944-3994/1944-3986
doi: 10.1080/19443994.2012.672204
Taylor & Francis
Taylor & Francis Group

Design optimization of ultrafiltration membrane module for desalination applications

Yun-Jin Kim[a], Taekgeun Yun[a], Jihee Han[a], Sangho Lee[a,*], Pyung-Kyu Park[b], Byung-Kook Hwang[b], Jong-Sang Park[b]

[a]*School of Civil and Environmental Engineering, Kookmin University, Jeongneung-Dong, Seongbuk-Gu, Seoul 136-702, Republic of Korea*
Tel. +82 2 910 4529; Fax: +82 2 910 4939; email: sanghlee@kookmin.ac.kr
[b]*Samsung Cheil Industries Inc., 332-2, Gocheon-Dong, Uiwang-Si, Gyeonggi-Do 437-711, Republic of Korea*

Received 25 December 2011; Accepted 10 February 2012

ABSTRACT

Ultrafiltration (UF) membrane provides an effective means of removing particles and microbial contaminants by size exclusion with the requirement of smaller footprints with conventional pretreatment processes. Although a few works have been done to optimize UF membrane modules and systems for drinking water treatment and membrane bioreactor (MBR), little information is available on UF design for pretreatment of seawater/brackish water desalination. This study focuses on the design of hollow fiber UF membrane modules for pretreatment processes in desalination plants. A theoretical model was developed and applied to predict the filtration efficiency of hollow fiber UF membranes. Typical conditions for pretreatment of feed solution to reverse osmosis desalination were considered. The effect of module dimensions and fiber packing density on pressure drops was also analyzed using the model. It was found that fiber thickness and module size are important as well as inner diameter and length of the fiber.

Keywords: Desalination; Pretreatment; Ultrafiltration; Module; Design; Optimization

1. Introduction

As available water sources are gradually depleted due to water scarcity as well as quality deterioration, seawater desalination has been gaining popularity as a feasible option for sustainable water supply [1,2]. High pressure reverse osmosis (RO) processes have been the technology of choice for seawater desalination [3,4]. RO has many advantages over other desalination techniques, including low energy requirements, low operating temperature, small footprint, modular design, and low water production costs. However, a stringent pretreatment is required to ensure high performance of RO membranes.

The use of microfiltration or ultrafiltration (MF/UF) has been studied by researchers since the mid-1990s and cost reduction in these technologies in the mid-2000s led to the installation of MF/UF pretreatment in seawater desalination plants [5]. The cumulative capacity will approach 9,000,000 m^3/d by the end of 2012, with annual installed capacities to exceed 2,000,000 m^3/d. The single largest pretreatment capacity currently contracted (Magtaa Seawater Desalination Plant in Algeria) requires over 1,000,000 m^3/d of pretreatment membrane capacity [6].

*Corresponding author.

It is well known that the efficiency of hollow fiber MF/UF modules depends on the fiber/module dimensions and operating conditions [7]. Thus, a few works have been done to optimize MF/UF membrane modules and systems for drinking water treatment and membrane bioreactor (MBR) [7–10]. However, little information is available on UF design for pretreatment of seawater/brackish water desalination. In case of UF pretreatment for RO desalination, a pressure-type module is preferred, while previous researchers have mostly focused on the optimization of submerged MF/UF modules.

This study focuses on the design of hollow fiber UF membrane modules for pretreatment processes in desalination plants. A theoretical model was applied to analyze the filtration efficiency of hollow fiber UF membranes. The effect of module dimensions and fiber packing density on fouling rate was examined using the model. Although this study was originally intended to design a membrane module for pretreatment of RO desalination, the findings may be applied to the similar applications, including wastewater reclamation and potable water treatment.

2. Theory

We have applied the hydrodynamic model equations for pressure drop outside and inside hollow fibers to predict the performance of dead-end UF over a wide range of conditions. Fig. 1 shows the flow and geometry in a hollow fiber UF membrane module. The feed flows inside the shell of the module, and the permeate flows inside the fibers. The permeate outlet and the feed inlet are at opposite ends of the module. The feed and permeate flow rates are identical since the module operates in the dead-end mode.

In this module, there are two kinds of pressure drop by water flows. In the shell side, a longitudinal pressure drop is created by the feed flow in the bundle of hollow fibers [11]. Accordingly, the pressure distribution in the shell side is given by [10]:

$$\frac{dp_s(x)}{dx} = -\frac{8\eta g(\varepsilon)}{\pi\varepsilon d_m^2 d_h d_o} Q_s(x) \tag{1}$$

where p_s is the shell-side pressure; x is the distance from feed inlet; η is the viscosity of water; g(ε) is the sparrow function; d_m is the inner diameter of the module; d_h is the hydraulic diameter; d_o is the outer diameter of the fiber; and Q_s is the feed flow rate in the shell side.

The pressure drop within a hollow fiber is given by the Hagen–Poiseuille law [9]:

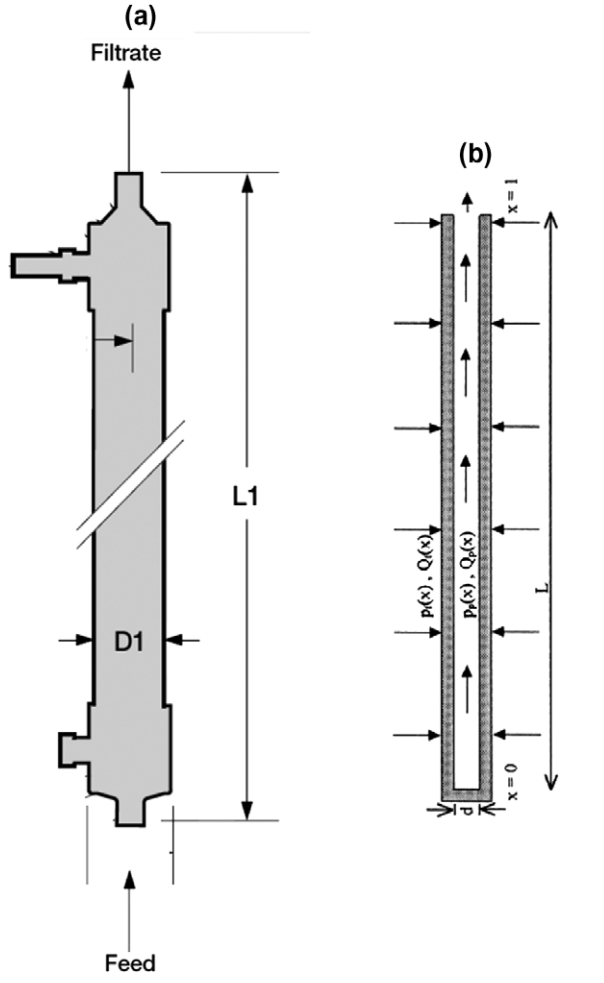

Fig. 1. Sketch of the flow and geometry in a hollow fiber UF membrane module: (a) module geometry and (b) flows outside and inside a fiber.

$$\frac{dp_f(x)}{dx} = -\frac{128\eta}{\pi d_i^2} Q_f(x) \tag{2}$$

where p_f is the pressure inside the hollow fiber; d_i is the inner diameter of the fiber; and Q_f is the permeate flow inside the fiber. Since dead-end filtration is assumed, the permeate flux is given by:

$$\frac{dQ_s(x)}{dx} = \frac{dQ_f(x)}{dx} = -n\pi d_o J(x) \tag{3}$$

where J is the local flux.

When the feed liquid is clean water, the above system of equations has an analytical solution. The local flux is given by the following equations [10]:

$$p(x) = (p_s(x) + p_f(x)) = \frac{((\alpha\cosh(\gamma L_f) + \beta)\cosh(\gamma x) + (\alpha\sinh(\gamma L_f))\sin(\gamma x))(\alpha + \beta)}{(\alpha^2 + \beta^2)\cosh(\gamma L_f) + \alpha\beta(2 + \gamma L_f \sinh(\gamma L_f))} \tag{4}$$

$$\alpha = \frac{8\eta g(\varepsilon)}{\pi\varepsilon d_m^2 d_h d_o} \tag{5}$$

$$\beta = \frac{128\eta}{\pi d_i^2} \tag{6}$$

$$\gamma = \sqrt{\left(\frac{8\eta g(\varepsilon)}{\pi\varepsilon d_m^2 d_h d_o} + \frac{128\eta}{\pi d_i^2}\right)\frac{n\pi d_o}{\eta R_m}} \tag{7}$$

where L_f is the effective fiber length. In order to consider pressure drop through the potting part, the Hagen–Poiseuille law may be applied:

$$p_{pot} = -\frac{128\eta L_{pot}}{\pi d_i^4} Q_f|_{x=L_f} \tag{8}$$

where L_{pot} is the length of the potting part. Thus, the average permeate flux, J_{avg}, is given by:

$$J_{avg} = \int_0^{L_f} J(x)dx = \int_0^{L_f} \frac{p_s(x) + p_f(x) + p_{pot}}{\eta R_m} dx \tag{9}$$

Due to the pressure drops in the shell side, fiber, and potting part, the permeate flux from Eq. (9) is different from the ideal flux calculated from the membrane resistance. Thus, the ratio of the permeate flux in the module to the ideal flux is used to quantify the efficiency of module design, which is defined as:

$$\lambda = \frac{J_{avg}}{J_{ideal}} = \frac{\int_0^{L_f} \frac{p_s(x)+p_f(x)+p_{pot}}{\eta R_m} dx}{\frac{\Delta P}{\eta R_m}} = \int_0^{L_f} \frac{p_s(x) + p_f(x) + p_{pot}}{\Delta P} dx \tag{10}$$

where ΔP is the applied pressure.

The above equations were simultaneously solved using Matlab. After solving the set of equations, the flux and the ratio of the calculated flux using the model to ideal flux were compared under various conditions.

3. Results and discussion

3.1. Local pressure and flux distribution

To begin, the local distributions of transmembrane pressure and permeate flux were estimated using the model as shown in Fig. 2. For this calculation, d_i was 700 μm and d_o was 1,300 μm, which are similar to commercially-available hollow fiber UF membranes. Due to pressure drop inside the fiber, the transmembrane pressure at the end of the fiber is lower than that at the outlet of the permeate, which results in a difference in the local flux along the fiber. Although the average flux is 171 L/m² h, the local flux is lower than 50 L/m² h in approximately 50% of the fiber. This suggests that the pressure drop inside the fiber may be substantial and affect the overall efficiency of the membrane filtration.

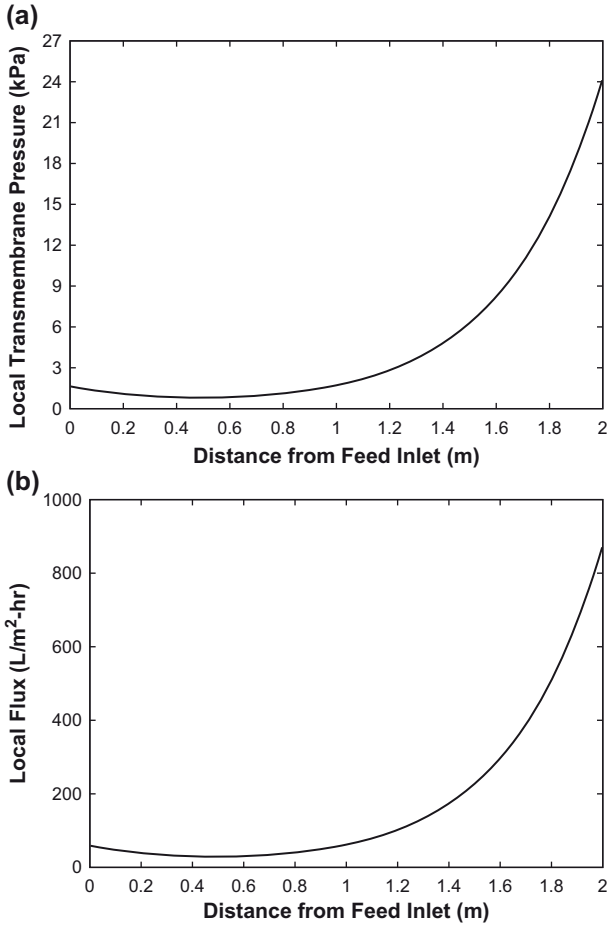

Fig. 2. Variations of local transmembrane pressure and flux with x position. Modeling conditions: d_i = 700 μm; d_o = 1,300 μm; A_m = 75 m²; d_m = 8 inch; T = 20°C; L_f = 2 m; L_{pot} = 0.3 m; $R_m = 10^{11}$ m^{-1}; Δp = 50 kPa. (a) Local transmembrane pressure. (b) Local flux.

Fig. 3 shows the local transmembrane pressure and permeate flux at d_i = 1,400 μm and d_o = 2,300 μm. Since the d_i is larger than the previous one, the pressure drop in the lumen side is smaller. Nevertheless, the larger d_o leads to higher packing density, resulting in an increase in the shell-side pressure drop. Accordingly, the local transmembrane pressure and the flux at the feed inlet are larger than those at the permeate outlet.

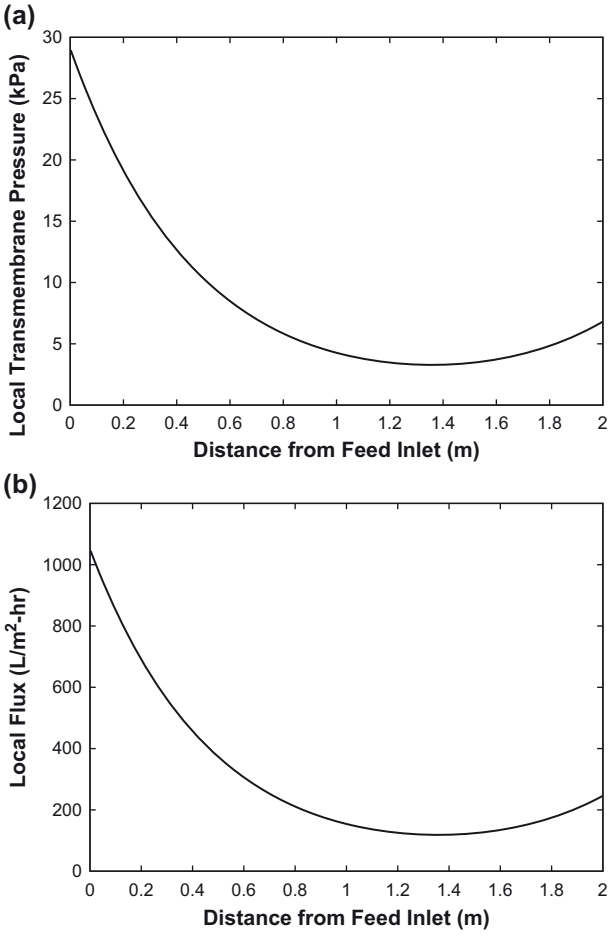

Fig. 3. Variations of local transmembrane pressure and flux with x position. Modeling conditions: $d_i = 1{,}400\,\mu m$; $d_o = 2{,}300\,\mu m$; $A_m = 75\,m^2$; $d_m = 8$ inch; $T = 20°C$; $L_f = 2\,m$; $L_{pot} = 0.3\,m$; $R_m = 10^{11}\,m^{-1}$; $\Delta p = 50\,kPa$. (a) Local transmembrane pressure. (b) Local flux.

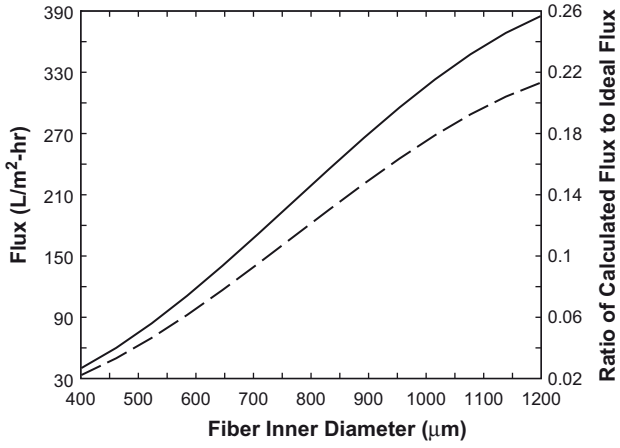

Fig. 4. Dependence of average flux and the ratio of calculated flux to ideal flux on the inner diameter of fiber at fixed membrane thickness. Modeling conditions: $\delta = 600\,\mu m$; $A_m = 75\,m^2$; $d_m = 8$ inch; $T = 20°C$; $L_f = 2\,m$; $L_{pot} = 0.3\,m$; $R_m = 10^{11}\,m^{-1}$; $\Delta p = 50\,kPa$ (—: flux, - -: ratio of calculated flux to ideal flux).

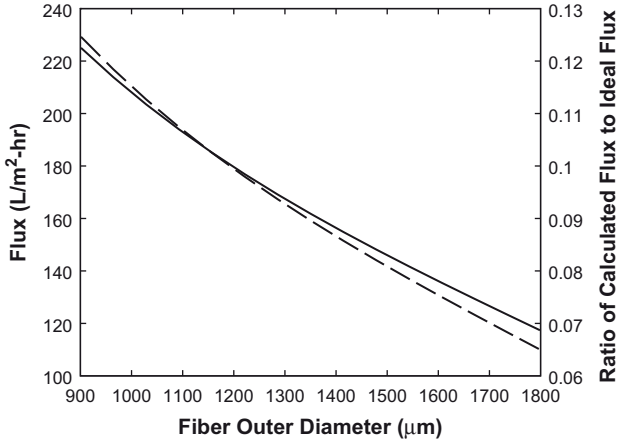

Fig. 5. Dependence of average flux and the ratio of calculated flux to ideal flux on the outer diameter of fiber at fixed inner diameter. Modeling conditions: $d_i = 900\,\mu m$; $A_m = 75\ m^2$; $d_m = 8$ inch; $T = 20°C$; $L_f = 2\,m$; $L_{pot} = 0.3\,m$; $R_m = 10^{11}\,m^{-1}$; $\Delta p = 50\,kPa$. (—: flux, - -: ratio of calculated flux to ideal flux).

The average flux is estimated to $298\,L/m^2\,h$ and the ratio of the calculated flux to the ideal flux is 16%.

3.2. Effect of fiber dimensions

It is clear from the above results that the fiber dimensions such as d_i, d_o, and L_f are important factors affecting the performance of a UF membrane module. Fig. 4 illustrates the relationship between d_i and the flux as well as the module efficiency. The thickness of the fiber (δ) was fixed to 600 μm for this calculation. Although the membrane resistance is fixed at $10^{11}\,m^{-1}$, the flux increases from $32\,L/m^2\,h$ to $390\,L/m^2\,h$ as increasing d_i, which results in a reduced pressure drop in the lumen side. Moreover, the efficiency ratio increases from 2 to 22%. The d_o also increases as the δ is constant, but the shell-side pressure drop seems to be less important than the lumen-side pressure drop in this case.

Fig. 5 shows the effect of d_o on the flux and the efficiency ratio. In this case, d_i is fixed to 900 μm, implying that the lumen-side pressure drop is not significantly changed with d_o. Accordingly, the shell-side pressure drop dominates the changes in flux and efficiency ratio. As d_o increases from 900 to 1,800 μm, the permeate flux decreases from $225\,L/m^2\,h$ to $119\,L/m^2\,h$, which corresponds to approximately 50% reduction. This also suggests that pressure drop inside a UF

module is smaller at constant d_i with smaller membrane thickness. Nevertheless, it should be noted that decreasing the fiber thickness is not easy because it is related to its mechanical strength as well.

3.3. Effect of intrinsic membrane resistance

One of the key issues in membrane manufacturing is to develop technologies to improve membrane permeability or, in other words, reduce membrane hydraulic resistance. Fig. 6 shows how the flux and efficiency ratio change with membrane resistance. It is evident from the figure that a decrease in membrane resistance results in an increased flux. Nevertheless, the relationship is not linear. If the membrane resistance is over a certain value, its effect on the permeate flux is becoming less important. This is attributed to the fact that the permeate flux is determined not only by the membrane resistance but also the pressure drop inside the module. At high membrane resistances, the efficiency ratio approaches 1.0, indicating the effect of pressure drop is less important.

3.4. Effect of module geometry

As the module length increases, the pressure drops inside both shell side and lumen side increase. Thus, the flux and the efficiency ratio decreases with increasing the module length, as presented in Fig. 7. Nevertheless, a decrease in the module length leads to decreased membrane area per a UF module, thereby reducing the compactness of the overall system.

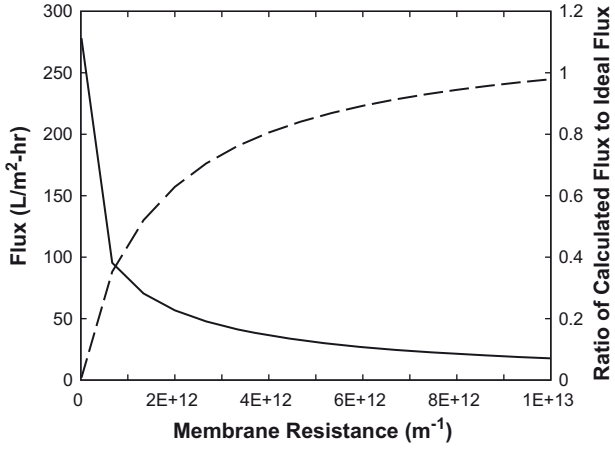

Fig. 6. Dependence of average flux and the ratio of calculated flux to ideal flux on membrane resistance. Modeling conditions: $d_o = 1{,}400\,\mu m$; $d_i = 700\,\mu m$; $A_m = 75\,m^2$; $d_m = 8$ inch; $T = 20°C$; $L_f = 2\,m$; $L_{pot} = 0.3\,m$; $\Delta p = 50\,kPa$ (—: flux, - -: ratio of calculated flux to ideal flux).

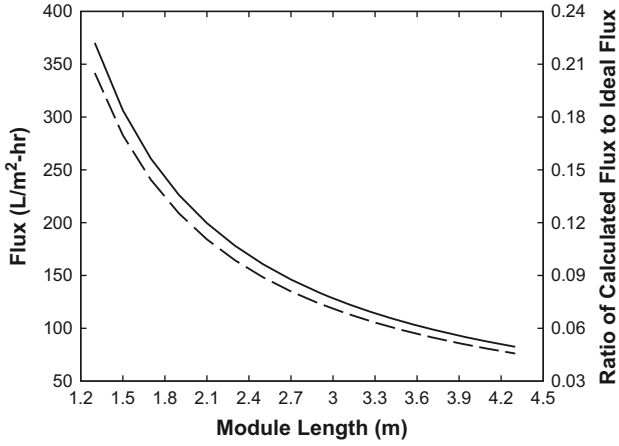

Fig. 7. Dependence of average flux and the ratio of calculated flux to ideal flux on module length. Modeling conditions: $d_o = 1{,}400\,\mu m$; $d_i = 700\,\mu m$; $d_m = 8$ inch; $T = 20°C$; $L_{pot} = 0.3\,m$; $R_m = 10^{11}\,m^{-1}$; $\Delta p = 50\,kPa$. (—: flux, - -: ratio of calculated flux to ideal flux).

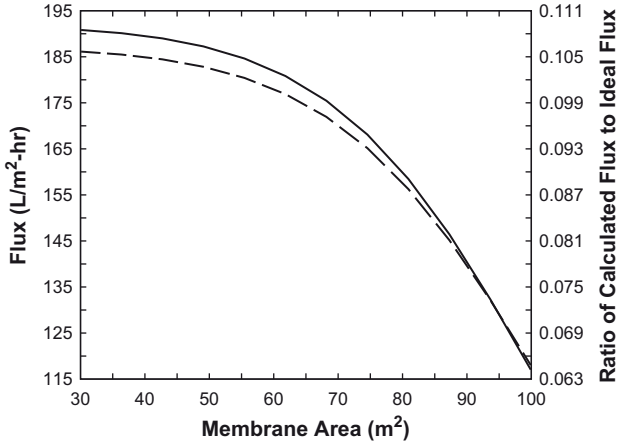

Fig. 8. Dependence of average flux and the ratio of calculated flux to ideal flux on the membrane area at fixed module diameter. Modeling conditions: $d_o = 1{,}400\,\mu m$; $d_i = 700\,\mu m$; $d_m = 8$ inch; $T = 20°C$; $L_{pot} = 0.3\,m$; $R_m = 10^{11}\,m^{-1}$; $\Delta p = 50\,kPa$. (—: flux, - -: ratio of calculated flux to ideal flux).

In the above simulation, the packing density is constant even with changing the module length. On the other hand, the results in Fig. 8 show how the packing density affects the flux and efficiency ratio by varying the membrane area. The module diameter was fixed at 8 inch for this calculation. As expected, the flux significantly decreases with the membrane area or the packing density.

In Fig. 9, the effect of module diameter was examined for two different membrane fibers: the first fiber

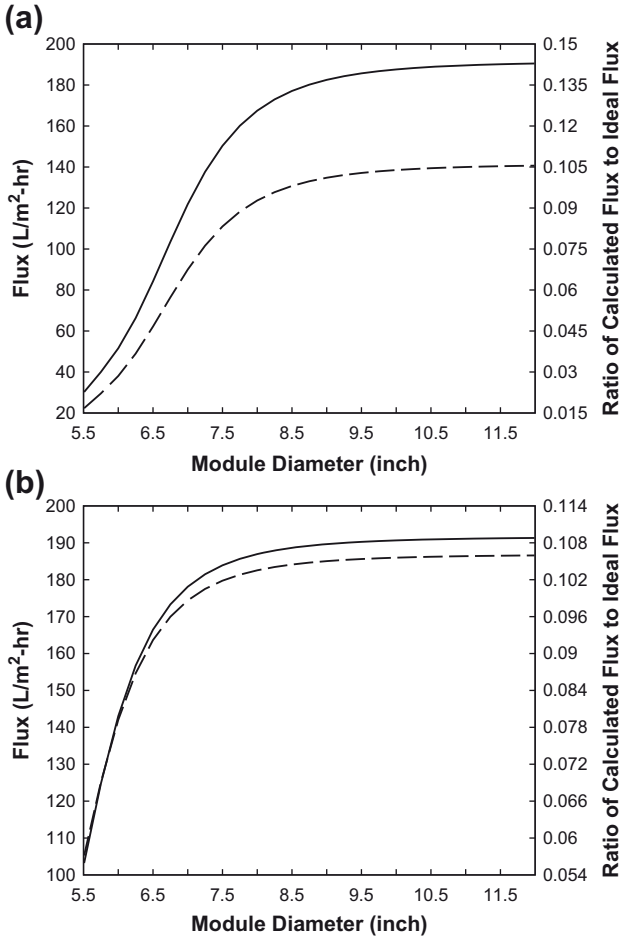

Fig. 9. Dependence of average flux and the ratio of calculated flux to ideal flux on module diameter. Modeling conditions: $T = 20°C$; $L_{pot} = 0.3$ m; $R_m = 10^{11}$ m^{-1}; $\Delta p = 50$ kPa. (—: flux, - -: ratio of calculated flux to ideal flux) (a) $d_o = 1{,}400$ μm and $d_i = 700$ μm (b) $d_o = 2{,}300$ μm; $d_i = 1{,}400$ μm.

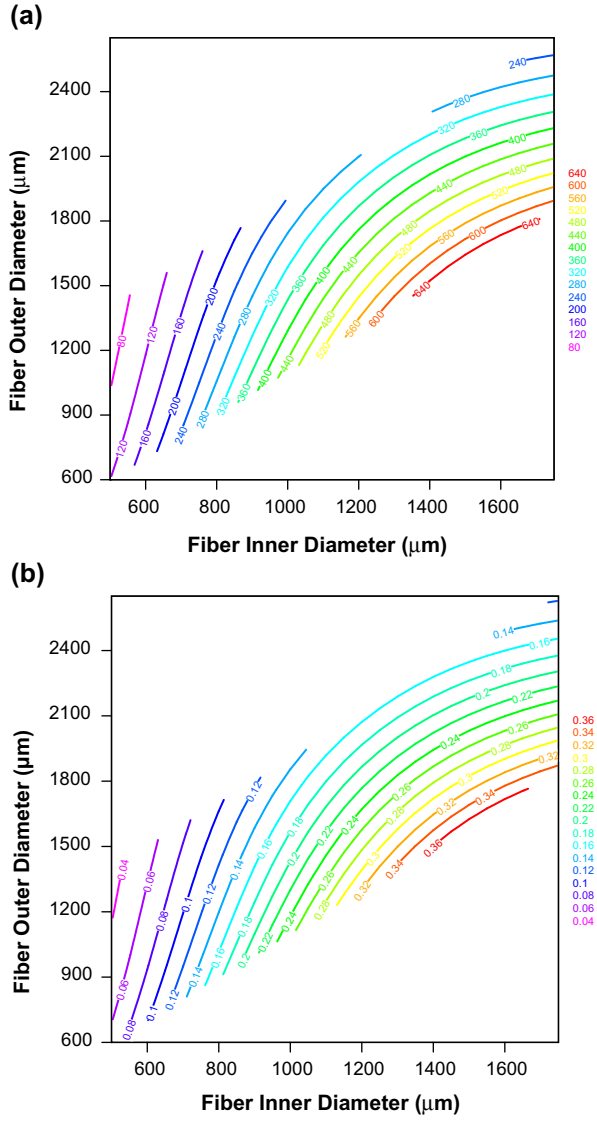

Fig. 10. Contour diagrams of average flux and efficiency ratio at different inner and outer diameters. Modeling conditions: $T = 20°C$; $L_{pot} = 0.3$ m; $R_m = 10^{11}$ m^{-1}; $\Delta p = 50$ kPa. (a) Average flux. (b) Efficiency ratio.

has $d_i = 700$ μm and $d_o = 1{,}400$ μm and the second fiber has $d_i = 1{,}400$ μm and $d_o = 2{,}400$ μm. Since the fiber with larger d_o results in a higher packing density, the optimum module diameter seems to be different for different d_o. For the first case, the optimum d_m appears to be 8 inch while the optimum one seems to be 7 inch for the second case.

3.5. Optimum fiber dimensions

To further investigate the effect of fiber dimensions on UF module performance, contours of constant flux and efficiency ratio are shown as a function of d_i and d_o. As shown in Fig. 10(a), the flux increases with d_i and decreases with d_o. At low d_i values, the effect of d_o is less significant since the lumen-side pressure drop is dominant. At high d_i values, the flux is becoming highly dependent on d_o due to increased shell-side pressure drop. Accordingly, the fiber with lower thickness is preferred for high flux UF membrane if possible. With the given conditions, the maximum efficiency ratio is 30% at $d_i = 1{,}500$ μm and $d_o = 1{,}700$ μm, as illustrated in Fig. 10(b).

Fig. 11 shows the average flux and efficiency ratio as a function of d_i and L_f. The membrane thickness is fixed at 500 μm and the membrane area per a module is proportional to the fiber length. The model calculations indicate that the flux increases as decreasing d_i and L_f. This graph can be used to determine the

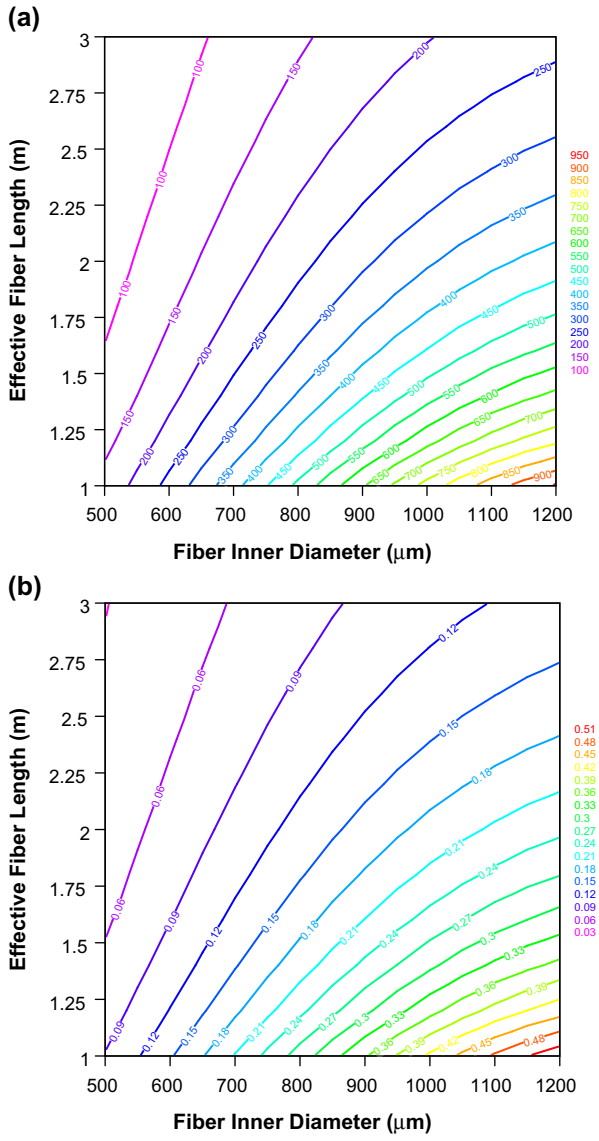

Fig. 11. Contour diagrams of average flux and efficiency ratio at different inner diameter and fiber length. Modeling conditions: $T = 20°C$; $L_{pot} = 0.3$ m; $\delta = 600$ μm; $R_m = 10^{11}$ m^{-1}; $p = 50$ kPa.

maximum fiber length for given fiber dimensions. For example, assuming that the efficiency ratio should be larger than 15%, the maximum fiber length at $d_i = 600$ μm is 1 m. At $d_i = 1{,}000$ μm, the maximum fiber length increases to 2.35 m.

In summary, the fiber dimensions of UF membrane should be determined by considering the lumen-side and shell-side pressure drops. It is desired to have small inner diameter and large outer diameter for reducing pressure drops. This eventually requires membranes with small fiber thickness, which is limited by the mechanical strength of the fiber. The fiber length should be determined to consider both lumen-side pressure drop and the compactness of the membrane module (or the unit membrane area).

4. Conclusions

In this work, theoretical analysis was carried out to optimize hollow fiber UF modules for the pretreatment of feed water to RO desalination plants under non-fouling conditions. Fiber thickness and module size are found to be important as well as inner diameter and length of the fiber. Of course, further works will be required to simulate UF membrane modules under fouling conditions.

Acknowledgments

This subject was supported by Korea Ministry of Environment as The Eco-Innovation project (Global Top project, Project no. GT-SWS-11-01-002-0).

References

[1] M. Wilf, C. Bartels, Optimization of seawater RO systems design, Desalination 173(1) (2005) 1–12.
[2] S.A. Avlonitis, K. Kouroumbas, N. Vlachakis, Energy consumption and membrane replacement cost for seawater RO desalination plants, Desalination 157(1–3) (2003) 151–158.
[3] H. Hyung, J.H. Kim, A mechanistic study on boron rejection by sea water reverse osmosis membranes, J. Membr. Sci. 286 (1–2) (2006) 269–278.
[4] S. Atkinson, Japan's largest sea-water desalination plant uses Nitto Denko membranes, Membr. Technol. 2005(4) (2005) 10–11.
[5] G.D. Profio, X. Ji, E. Curcio, E. Drioli, Submerged hollow fiber ultrafiltration as seawater pretreatment in the logic of integrated membrane desalination systems, Desalination 269 (2011) 128–135.
[6] R. Huehmer, Microfiltration/Ultrafiltration Pretreatment Trends in Seawater Desalination, The International Desalination Association, Perth, 2011.
[7] S.-H. Yoon, H.-S. Kimb, I.-T. Yeomb, Optimization model of submerged hollow fiber membrane modules, J. Membr. Sci. 234 (2004) 147–156.
[8] T. Carroll, N.A. Booker, Axial features in the fouling of hollow-fibre membranes, J. Membr. Sci. 168 (2000) 203–212.
[9] S. Lee, P.-K. Park, J.-H. Kim, K.-M. Yeon, C.-H. Lee, Analysis of filtration characteristics in submerged microfiltration for drinking water treatment, Water Res. 42 (2008) 3109–3121.
[10] C. Serra, M.J. Clifton, P. Moulin, J.-C. Rouch, P. Aptel, Dead-end ultrafiltration in hollow fiber modules: Module design and process simulation, J. Membr. Sci. 145 (1998) 159–172.
[11] E.M. Sparrow, A.L. Loeffler, Longitudinal laminar flow between cylinders arranged in regular array, AIChE J. 5 (1959) 325–330.